Hydride Reorientation in Zircaloy-4 Examined by In Situ Synchrotron X-ray Diffraction

H. E. Weekes[a], N. G. Jones[b], T. C. Lindley[a], D. Dye[a,*]

[a] *Department of Materials, Royal School of Mines, Imperial College London, Prince Consort Road, London, SW7 2BP, UK*
[b] *Department of Materials Science and Metallurgy, University of Cambridge, 27 Charles Babbage Road, Cambridge, CB3 0FS, UK*

Abstract

The phenomenon of stress-reorientation has been investigated using *in situ* X-ray diffraction during the thermomechanical cycling of hydrided Zircaloy-4 tensile specimens. Results have shown that loading along a sample's transverse direction (TD) leads to a greater degree of hydride reorientation when compared to rolling direction (RD)-aligned samples. The elastic lattice micro-strains associated with radially oriented hydrides have been revealed to be greater than those oriented circumferentially, a consequence of strain accommodation. Evidence of hydride redistribution after cycling, to α-Zr grains oriented in a more favourable orientation when under an applied stress, has also been observed and its behaviour has been found to be highly dependent on the loading axis. Finally, thermomechanical loading across multiple cycles has been shown to reduce the difference in terminal solid solubility of hydrogen during dissolution ($TSS_{D,H}$) and precipitation ($TSS_{P,H}$).

1. Introduction

Zirconium alloys are used extensively in structural applications in water reactor cores, due to their low neutron absorption, adequate strength at operating temperatures and corrosion resistance. At elevated temperatures, during reactor operation, these components are highly sensitive to hydrogen absorption as a result of aqueous corrosion. Whilst at operating temperature, ~600 K, hydrogen solubility in α zirconium is around 100 ppmw, on cooling to ambient temperature the solubility decreases to <20 ppmw[1]. This results in the precipitation of zirconium hydrides. As the hydrides are, themselves, brittle, their precipitation results in severe embrittlement of the accommodating zirconium metal component. To an extent, this is controlled by engineering the crystallographic texture of zirconium fuel cladding so as to promote the formation of circumferential hydride packets, as the hydrides have a preferred orientation relationship and habit plane with the matrix phase. During interim storage, or due to temperature fluctuations in service, stresses can be generated. This can occur due to fission gas release or fuel swelling and may lead to stress reorientation of the hydrides on cooling, Figure 1.

During dry storage, the maximum hoop stresses experienced by the cladding can reach 150 MPa, with typical values ranging from 100 to 120 MPa[2]. With the potential for temperatures to reach 673 K during the transfer of spent fuel rods from wet to dry storage the likelihood of already existing circumferential hydrides dissolving and re-precipitating parallel to the radial axis of the cladding is high. This is assuming the hoop tensile stress on the cladding is larger than a certain threshold stress, reported to be in the region of 70-100 MPa[3, 4]. As the temperature decreases from 673 K to ~473 K over the tens of years after shutdown, the cladding will mainly be operating in a regime of low hydride reorientation (<100 MPa, >473 K)[5]. Few factors have been reported to affect the threshold stress, namely alloy strength and residual stresses [6], whilst a multitude of factors are understood to affect the degree of radial hydride precipitation once this threshold has been reached. These include (i) temperature[7, 8], (ii) applied tensile hoop stress ($\sigma_{H,max}$)[3, 8, 9], (iii) hydride concentration ($C_{H,i}$)[7, 10], (iv) number of applied thermal cycles[10, 11] and (v) degree of cold-work[12, 13].

The most commonly observed hydride phase in fuel cladding, and the one considered throughout this study,

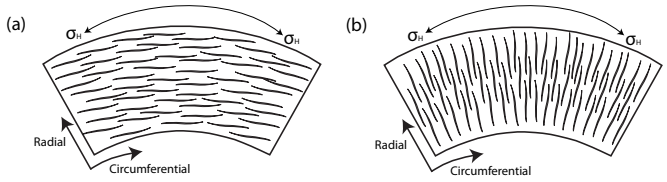

Figure 1: Schematic representation of hydride stress-reorientation where zirconium hydrides, when cooled under a tensile hoop stress above a certain threshold, reprecipitate along the radial direction of the cladding tube.

*Corresponding author.
Email address: david.dye@imperial.ac.uk (D. Dye)

is δ-ZrH_x, where 1.5 <x< 1.7, although occasional observations of the γ-ZrH_x and ϵ-ZrH_x, where x=1 and x=2 respectively, must be noted. δ-ZrH has an fcc crystal structure, with $a = 4.786$ Å, whilst the hcp α zirconium has lattice parameters of $a = 3.2276$ Å and $c = 5.1516$ Å. The orientation relationship between the δ-hydride and α-Zr has been found to be δ-$ZrH_{(111)} \| \alpha$-$Zr_{(0002)}$ and δ-$ZrH_{[1\bar{1}0]} \| \alpha$-$Zr_{[11\bar{2}0]}$[14, 15].

The δ-Zr hydride precipitates as fine micro platelets, on the order of 50 nm in size, with a nominal $\{0002\}_{\alpha\text{-Zr}}$ habit plane. These sympathetically nucleate to form self-accommodating agglomerates termed hydride packets, around 14 ° from the basal plane, close to $\{10\bar{1}7\}_{\alpha\text{-Zr}}$. These strain fields give rise to a hysteresis in the precipitation and dissolution temperatures.The precipitation of these hydrides can be affected by the presence of stress fields, leading to reorientation of the hydride packets under stress on thermal cycling; the platelet orientation relationship is preserved but the packet morphology changes[16].

The majority of studies on hydride stress-reorientation have been carried out post-mortem using metallography to determine the change in hydride orientation after the application of a thermo-mechanical cycle. The technological goal has been to establish the interplay of the extent of reorientation, the effect of irradiation and cold work, stress and temperature. Recently, Colas et al [3, 17] have examined reorientation using synchrotron X-ray diffraction. It was observed that the hydride peak intensities (texture) did not change on reorientation, but that some of the peak widths could be observed to change, as a consequence of the rearrangement of the strain and defect distributions around the hydrides on dissolution and re-precipitation.

In the present work, this phenomenon has been further explored, examining the effect of loading in different texture directions of the α-Zr material, the effect of multiple cycles and of threshold stresses that relate to those expected in dry storage, at moderate hydride concentrations. The material used was annealed and relatively coarse grained Zircaloy-4, a lightly-alloyed zirconium alloy, acting as a comparator to work on heavily cold worked thin-walled fuel tube material.

2. Experimental

2.1. Sample Preparation

The Zircaloy-4 tested was obtained from a 10mm hot rolled sheet supplied by Rolls-Royce plc. Tensile specimens were designed and fabricated, Figure 2. Rectilinear blanks were removed from the Zircaloy-4 plate and electrolytically charged with hydrogen in a dilute sulphuric acid solution (1% H_2SO_4) using a current density of $\sim 2\,kAm^{-2}$. Immersion of samples in a diluted HF/HNO_3 solution (1% HF, 1%HNO_3) preceded hydrogen charging in order to remove any surface oxide, which can impede hydrogen ingress into the bulk. Diffusion of the hydride layer into the bulk to form uniformly distributed hydrides was obtained *via* a

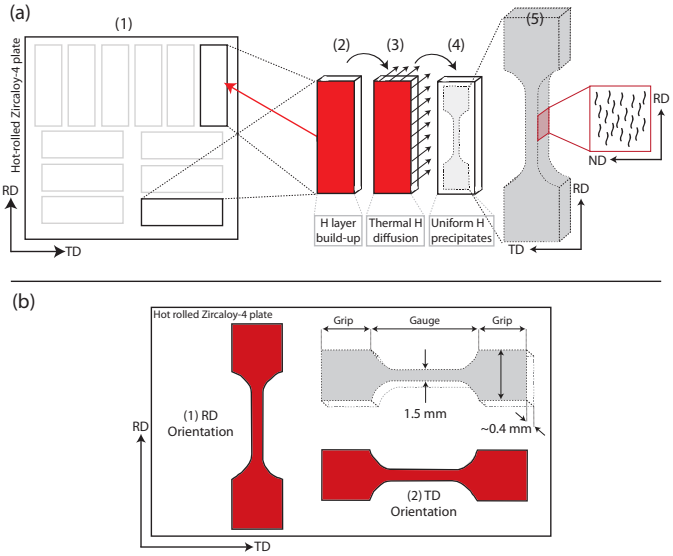

Figure 2: (a) Sample fabrication process. (1) Blanks removed from the bulk Zircaloy-4 plate using electro discharge machining (EDM), (2) Surface hydride layer produced via electrochemical charging, (3) Application of thermal anneal to diffuse hydrogen into bulk, (4) Uniformly distributed hydride precipitates aligned along sample RD and (5) Final sample, (b) Illustration of the two dogbone orientations used during data collection (1) RD (2) TD.

thermal treatment whose temperature was governed by the assumed hydrogen solubility. A slow furnace cool was used to promote the formation of stable δ zirconium hydrides. Once hydrided, dogbone-shaped tensile test-pieces were fabricated and two orientations were tested; (1) rolling direction (RD) parallel to the loading axis and (2) transverse direction (TD) parallel to the loading axis. The crystallographic texture of the starting Zircaloy-4 material aligns the basal poles near to the sample normal direction (ND) ($\pm\sim 30°$)[18]. Macroscopic hydride 'stringers' are readily observed, a result of the tendency for individual micro-hydride platelets to autocatalytically nucleate to form what appears to be a larger hydride packet. The hydrogen concentration for all samples has been estimated to be 280 ($\pm$30) ppmw, from the hydride layer thickness during charging and from the dissolution temperatures found during the diffraction experiments on heating.

2.2. Metallography

Samples were examined before and after cycling in order to quantify the hydride packet orientations. This was carried out using backscattered electron imaging (BSE), exploiting the compositional contrast between the matrix and hydride phases. Electron imaging of polished samples is often preferred to the examination of acid etched material, as etching can give rise to apparent changes in the size and morphology of the hydrides. This effect has been demonstrated using secondary electron imaging of the cross-section of an embedded hydride, Figure 3(a-b). The trench was milled using a focused ion beam (FIB).

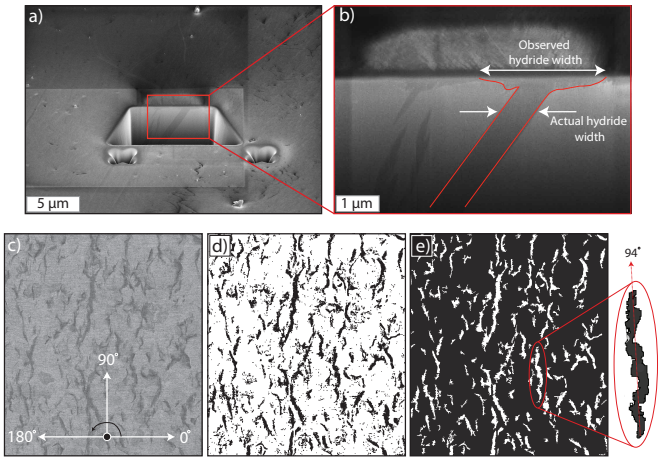

Figure 3: Secondary electron (SE) images showing the overestimation of hydride size at the sample surface due to chemical etching. (a) FIB-milled trench showing the hydride cross-section below the sample surface and (b) higher magnification SE image of an intragranular hydride, showing an increase in the apparent width at the sample surface, (c-e) BSE, binary and binary-outlined images used to establish hydride orientations before and after loading.

The method used to establish individual hydride packet orientations is outlined in Figure 3(c-e). The image analysis software ImageJ was used to convert the BSE images into binary images using a greyscale threshold limit. Individual hydride packets were then identified, fitted with an ellipsoid, and their orientation assessed, with 0° being assigned as the direction perpendicular to the loading axis. This preceded the construction of frequency distributions of the macroscopic hydride packet orientations.

EBSD was carried out on as-received Zircaloy-4 to determine the crystallographic texture and grain size of the starting material. Samples were ground using SiC paper and electropolished using a mixture of 10% perchloric acid and 90% methanol at a voltage of 30V and temperature of -30°C.

2.3. Synchrotron Diffraction and Data Analysis

Synchrotron X-ray diffraction was carried out on hydrided Zircaloy-4 test pieces in conjunction with the application of a thermomechanical load cycle. A schematic of the set up is shown in Figure 4. Samples were heated using infrared heaters under a tensile stress of ∼30 MPa to 550 °C and held for ∼ 10 min in order to ensure full dissolution of the hydride precipitates. A larger tensile stress was applied at the start of cooling, which was carried out at a rate of 0.2 °C s^{-1}. This slow cool ensured heterogeneous nucleation of the δ zirconium hydride phase once the terminal solid solubility temperature for precipitation ($TSS_{P,H}$) was reached. The temperature was controlled using a Eurotherm controller and monitored using K-type thermocouples. For all samples cooled under an applied load, 30 MPa was applied during heat-up and hold. This was not applied at any point across the cycle for the samples cooled under no load. Full Debye-Scherrer diffraction rings were collected continuously using a monochromatic X-ray beam of energy 80 keV (λ=0.15487 Å) on a large (2880 × 2881 pixel) Pixium 2D area detector at a sample-to-detector distance of ∼1600 mm. To allow for improved grain sampling, the stage was incrementally rotated in 0.5° steps, with a full rotation equating to ±5°. A diffraction pattern was recorded at each step.

During data analysis, the collection of 2D images obtained from each rotation series were averaged in order to form a single diffraction pattern. Using Fit2D, the full diffraction rings were integrated across a single angular range (±10°) around the direction corresponding to

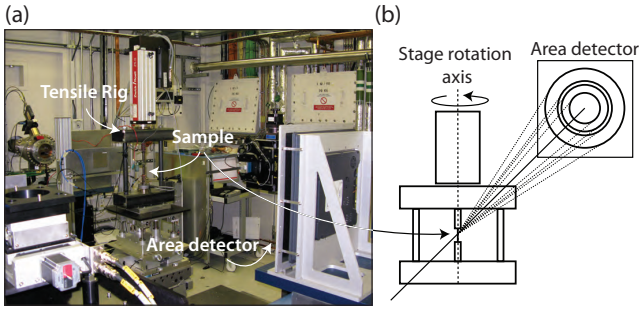

Figure 4: (a) Diamond I12 beamline showing the tensile rig set-up for hydride reorientation experiments and (b) schematic of rig showing stage rotation axis and generated diffraction rings from a polycrystalline sample.

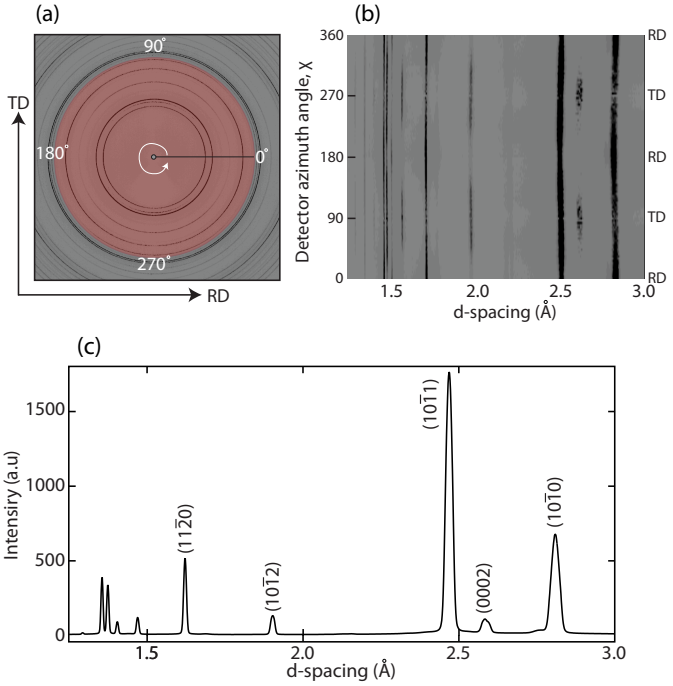

Figure 5: (a) An example of a generated diffraction pattern showing a full set of Debye Scherrer rings, (b) an 'unwrapped' diffraction plot and (c) the corresponding diffraction pattern, obtained from a TD sample after a full 360° ring integration.

the loading axis. Diffraction signals termed 'TD' were obtained from the crystallographic planes with normals parallel to the transverse direction ($\pm 10°$) while those from the RD were from those planes with their normals parallel to the rolling direction ($\pm 10°$). The wavelength, beam centre and detector tilt were determined using a ceria (CeO_2) standard at two sample-to-detector distances.

Figure 5 shows an example of the diffraction data processing. Figure 5(a) shows a full diffraction ring plot generated from a TD aligned sample, emphasising the full 360° azimuthal integration used to produce the accompanying plots. Figure 5(b) shows the diffraction pattern processed to 'unwrap' the diffraction rings, allowing peak shifts to be visualised. The corresponding conventional intensity-d_{hkil} diffraction pattern for the complete ring integration is also shown in Figure 5(c). Individual hydride reflections were fitted using a Gaussian in IgorPro, along with an appropriate background and doublet description, allowing the evolution of their integrated intensity, peak width (full width half maximum) and peak position to be followed. These three quantities are independent in the fitting, and therefore can be interpreted independently of each other.

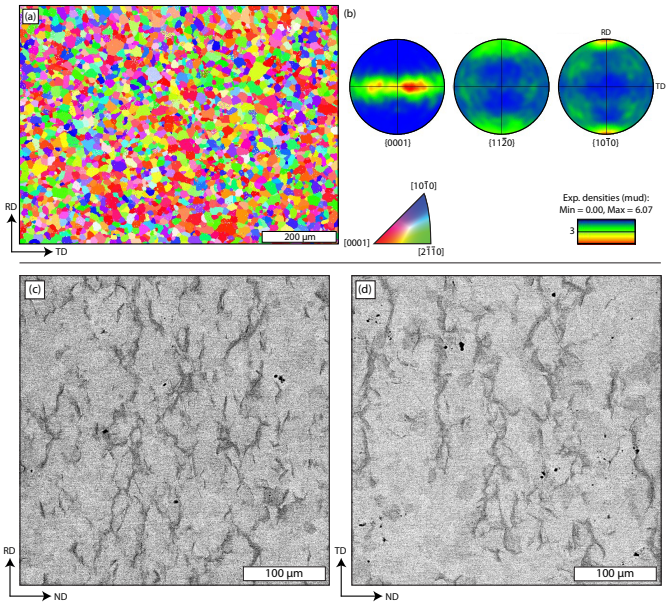

Figure 6: (a) EBSD map of the as-received Zircaloy-4, (b) the corresponding pole figures highlighting the expected rolling texture. (Map size: 675×860 µm, step size: 1.5 µm, number of grains: 8082), (c-d) BSE images showing uniformly dispersed hydride packets, post diffusion annealing, for an RD (a) and TD (b) aligned sample showing their orientation relative to the sample ND.

3. Results

3.1. Sample Characterisation

The initial Zircaloy-4 microstructure was single α phase, composed of equiaxed grains with an average grain size of 20 µm (established using EBSD, Figure 6). The $\{0002\}_{\alpha\text{-Zr}}$ pole figure shows two distinct maxima in basal pole density, close to the sample ND, with the <*a*> directions along the RD. The calculated Kearns factors for the starting material are presented in Table 1 and are in good agreement with previous reported values[13, 19, 20]. Figure 6(c-d) shows the hydride packet habit plane normals were parallel to the plate ND (or, equivalently, the trace of the habit plane in the TD-RD plane), as expected. The hydride dispersion was observed to be uniform throughout each sample cross-section. Figure 6(c-d) compares the degree of hydride alignment and connectivity when viewed along the sample RD (c) and TD (d).

3.2. Effect of thermomechanical cycling on hydride orientation

The effect of a single thermomechanical cycle on the macroscopic orientation of the hydride packets is shown in Figure 7. In the example presented, the applied load on cooling was 100 MPa, and a loading direction parallel to the RD (left) is compared to a loading direction parallel to the TD (right). Prior to cycling, both samples showed preferential hydride alignment, with the majority of the hydride packet traces at inclinations $> 60°$ away from the ND, *i.e.* with the packet normals close to the ND. After a single cycle, a distinct change from this preference was observed. A more random orientation distribution in the samples loaded along RD, and a slight preferential alignment towards the TD for the TD-loaded sample was observed.

Table 1: Calculated Kearns parameter for Zircaloy-4 sheet used during this study

Direction	f_{ND} (radial)	f_{RD} (axial)	f_{TD} (circumf.)
	0.56	0.05	0.39

The effect of varying the stress applied on cooling on the hydride packet orientation distributions are shown in Figure 8. For all samples cooled under an applied load, 30 MPa was applied during heat-up and hold. This was not applied at any point across the cycle for the samples cooled under no load. Figure 8(a-b) schematically represents the angular ranges used when characterising hydride orientations. Appealing to the orientation distributions that would pertain for typical fuel tube textures, with $\{0002\}_{\alpha\text{-Zr}}$ parallel to the radial direction, hydride packet traces at angles near-90° to the $\{0002\}_{\alpha\text{-Zr}}$ texture (ND in the present plate) would lie circumferentially. In the fuel tube literature [21], angles of $0 - 40°$ are then termed 'radial hydrides', and $40 - 65°$ are termed 'mixed'.

For RD-aligned samples, as the applied stress increased, the fraction of hydride packets with their normal along ND (65-90°) gradually decreased, whilst a larger effect was observed for loading along TD. The case of no-load thermal cycling is also shown for reference. For the TD-aligned sample, the fraction of 'radial' hydrides (0-40°) were found

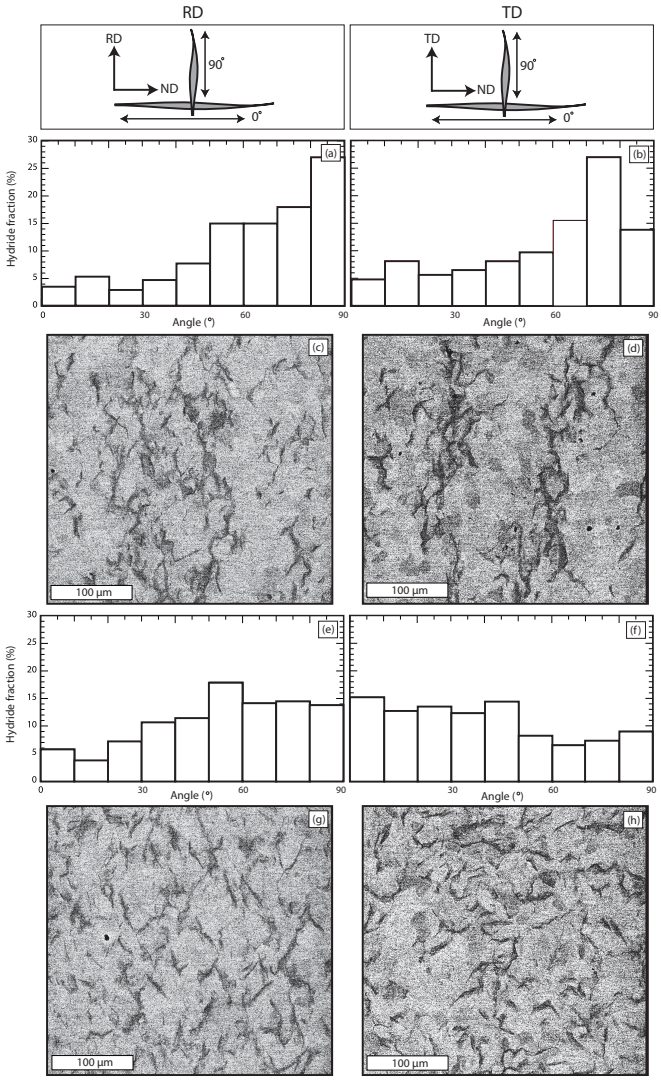

Figure 7: Effect of 100 MPa stress during cooling on the hydride packet orientations observed using BSE microscopy. (left) RD and (right) TD. (a-d) before testing, (e-h) after thermomechanical cycling. (a-b) and (e-f) show the corresponding fitted packet orientation distributions.

to increase to as high as $\sim$ 55% for an applied stress of 100 MPa, while the fraction of 'mixed' hydrides (40-65°) remained approximately constant. A distinct threshold was not observed.

3.3. In situ synchrotron diffraction

3.3.1. Single thermomechanical cycle

In situ diffraction experiments were carried out during the thermomechanical cycling of four hydrided Zircaloy-4 samples charged to a hydrogen level of $\sim$280 ppmw. Figure 9(a) shows a full-ring azimuthally integrated diffraction pattern obtained from an RD-aligned sample, highlighting the locations of the $\{111\}_{\delta\text{-ZrH}}$ and $\{220\}_{\delta\text{-ZrH}}$ peaks.

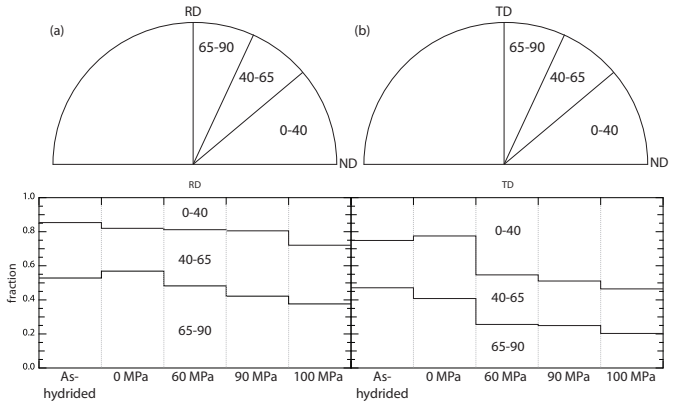

Figure 8: Distribution of hydride orientation, relative to the axis of loading, after undergoing a single thermomechanical cycle, when cooled under different applied loads. (a) loading axis ∥ RD, (b) loading axis ∥ TD.

The evolution of both hydride peaks during a full thermomechanical cycle is shown in Figure 9(b-c). The dissolution and precipitation of the δ hydride correlates to the regions of increasing and decreasing peak intensity. The temperature corresponding to the $\text{TSS}_{\text{D,H}}$ (red) was assigned to the temperature at which the hydride peaks were no longer visible in the diffraction patterns, whilst $\text{TSS}_{\text{P,H}}$ (blue) refers to the temperature at which the hydride phase was first observed upon re-precipitation into the matrix on cooling. Table 2 presents the dissolution ($\text{TSS}_{\text{D,H}}$) and precipitation ($\text{TSS}_{\text{P,H}}$) temperatures, along with the corresponding hydrogen concentrations for all samples. The observed hysteresis in solubility is a result of varying internal stresses, and associated plastic deformation, dependent upon whether hydrides are forming from or dissolving into the matrix. The $\text{TSS}_{\text{D,H}}$ and $\text{TSS}_{\text{P,H}}$ were determined using the solubility equations in [22] and the average hydrogen level quoted was obtained from the dissolution temperatures. The estimated uncertainties in the dissolution and precipitation temperatures were 14 and 8°C respectively.

Figures 10 and 11 compare the evolution of the $\{111\}_{\delta\text{-ZrH}}$ and $\{220\}_{\delta\text{-ZrH}}$ peaks during a single thermomechanical cycle across an azimuthal angular range ±10° to the axis of loading. The integrated intensity is shown, normalised

Table 2: Dissolution and precipitation temperatures obtained from synchrotron X-ray diffraction. The implied hydrogen concentration in the Zircaloy-4 samples is also given, obtained from TSSD and TSSP and the equations in [22]. In each case, the implied H concentration obtained by electrolytic charging was around 300 ppmw.

Sample	$\text{T}_{\text{Diss.}}$ (°C)	$\text{T}_{\text{Precip.}}$ (°C)	TSSD (ppmw)	TSSP (ppmw)
100 MPa TD	460	408	290	315
100 MPa RD	471	420	316	350
0 MPa TD	442	391	250	270
0 MPa RD	452	411	272	323

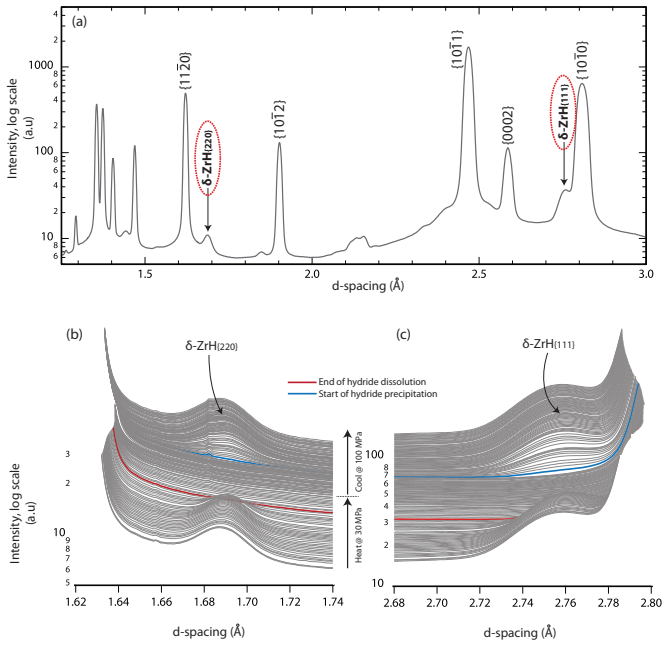

Figure 9: (a) Full-ring azimuthally integrated diffraction pattern from an RD oriented Zircaloy-4 sample charged with ∼250 ppmw H. (b-c) waterfall plots of δ-ZrH$_{\{220\}}$(b) and δ-ZrH$_{\{111\}}$(c) showing their evolution during a single thermomechanical cycle.

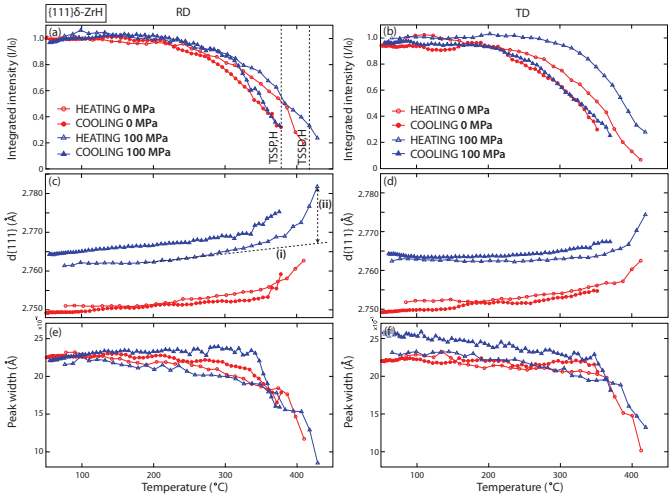

Figure 10: Evolution of the δ-ZrH$_{\{111\}}$ peak, within ±10° of the loading direction, during thermomechanical cycling with applied stress on cooling of 0 and 100 MPa. The variation in normalised integrated intensity, I/I$_0$ (a-b), peak position, d$_{\{111\}}$ (c-d) and peak width, FWHM/1.665 (e-f) are shown. (left) RD sample, (right) TD.

against the intensity at the beginning of the thermal cycle for that sample. Both hydride peaks in both the RD and TD-aligned samples show the expected hysteresis in peak intensity on dissolution and re-precipitation (where TSS$_{D,H}$>TSS$_{P,H}$[22]) was observed, Figures 10(a-b) and 11(a-b). In terms of the hydride peak intensity values, no significant changes are observed for either the $\{111\}_{\delta\text{-ZrH}}$ or $\{220\}_{\delta\text{-ZrH}}$ during either load cycle (0/100 MPa).

Turning to the evolution in $\{111\}_{\delta\text{-ZrH}}$ lattice parameters, d$_{\{111\}}$ in Figure 10, a difference of ∼0.01 Å between both samples can be noted. This has been attributed to variation in the sample-to-detector distance between the experiments (see note below). On initial heating, d$_{\{111\}}$ can be seen to increase slightly, associated with constrained thermal expansion, indicated (i). Further heating, completing the dissolution process, resulted in a more rapid change in d$_{\{111\}}$ (ii). This is suggested to be a consequence of the release of misfit strains between the matrix and hydride phases. Figure 11 presents the corresponding data for the $\{220\}_{\delta\text{-ZrH}}$ peak; rapid changes in its peak position during dissolution and re-precipitation are not observed, and in some cases a slight reduction in strain as the hydride approaches full dissolution is seen to occur (d). In general, this behaviour is consistent for both RD and TD-aligned samples.

On completion of a single cycle when cooled under stress, both samples showed a positive change in d$_{\{111\}}$, more noticeable in the RD-aligned samples, Figure 10. This is suggestive of a change in stress distribution in the hydrides associated with their (partial) reorientation. Similar behaviour can be observed for the d$_{\{220\}}$ peak for both RD and TD-aligned samples, Figure 11(c-d), when cooled under a load. Samples undergoing a simple heating/cooling cycle with no application of load showed a slight reduction in d$_{\{220\}}$.

The hydride peak widths plotted in Figure 10(e-f) for $\{111\}_{\delta\text{-ZrH}}$ and Figure 11(e-f) for $\{220\}_{\delta\text{-ZrH}}$, are simply the full width half maximum divided by $2\sqrt{\ln 2} = 1.665$. A steady decrease can be observed during dissolution, corresponding to a steady decrease in strain broadening. This change is gradual across the entire heating portion of the cycle. During initial re-precipitation into the matrix on cooling, the change in peak width was more abrupt. In general, higher peak widths were observed on cooling under load for the $\{111\}_{\delta\text{-ZrH}}$, in particular in the TD-oriented samples which showed a greater degree of reorientation. Similar behaviour was observed for the $\{220\}_{\delta\text{-ZrH}}$ peak during heating but there was a reduction in associated peak broadening during cooling.

Note on Experimental Errors

Typical fractional peak position, intensity and width fitting uncertainties were 1–2×10^{-4}, 0.5×10^{-3} and 0.5×10^{-3}, respectively. However, for absolute measurements of lattice parameters, additional sources of uncertainty must be considered. For lattice parameter, the positioning uncertainty of the sample in the beam is on the order of $\delta D = 0.3$mm, which relates to an angular uncertainty of $\delta D/D \simeq 2 \times 10^{-4}$, given the sample-to-detector distance used of $D = 1600$mm. This then translates directly into the fractional lattice parameter uncertainty - and so the initial lattice parameter of a given peak has a substantially higher (around double) sample-to-sample uncertainty than the statistical peak fitting uncertainty. Normalisation of the integrated intensity removes the effect of sample thick-

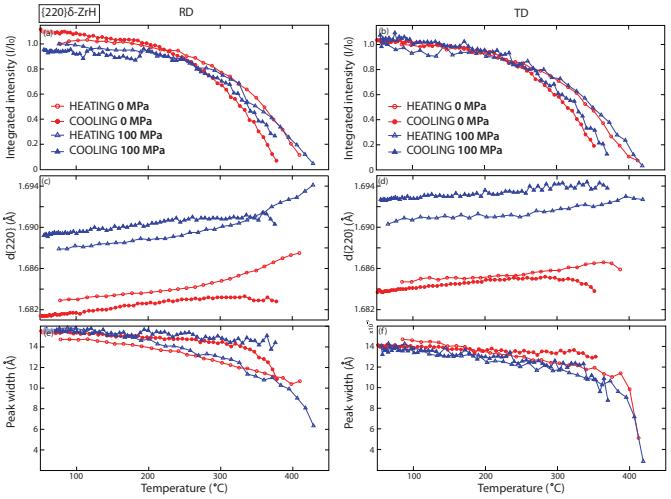

Figure 11: Evolution of the δ-ZrH$_{\{220\}}$ peak, within $\pm 10°$ of the loading direction, during thermomechanical cycling with applied stress on cooling of 0 and 100 MPa. The variation in normalised integrated intensity, I/I_0 (a-b), peak position, $d_{\{220\}}$ (c-d) and peak width, FWHM/1.665 (e-f) are shown. (left) RD sample, (right) TD.

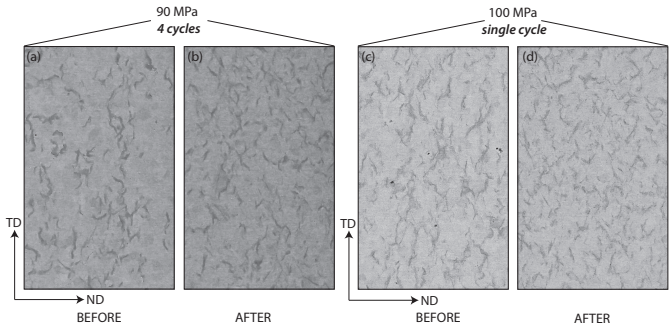

Figure 12: Backscattered electron micrographs before (a) and after (b) four thermomechanical cycles cooled under a 90 MPa tensile load and before (c) and after (d) a single thermomechanical cycle cooled under a 100 MPa tensile load. Both loading axes||RD.

ness variations, but is still vulnerable to texture variations owing to, for example, slight angular variations in the alignment of the sample, but this is small for the textures used.

3.3.2. Multiple thermomechanical cycles

Figure 12 compares BSE micrographs obtained from two RD-aligned samples before (a,c) and after (b,d) undergoing multiple (a-b) and single (c-d) thermomechanical load cycles. Both samples show similar reorientation behaviour, with the hydrides' long axis normal realigning close to 45° to the sample ND.

The evolution of the hydride peaks during repeated cycles is shown in Figure 13. Held at 30 MPa during heating, an RD sample was slowly cooled from a ten minute hold at 550°C under a tensile load of 90 MPa, as previously. This cycle was repeated four times.

First considering the change in peak intensity across all cycles, Figure 13(a,d), the hysteresis in hydrogen solubility between heating and cooling can be observed. After the first cycle, the difference between the $TSS_{D,H}$ and $TSS_{P,H}$ was shown to decrease and remained relatively constant thereafter. This behaviour was observed for both the $\{111\}_{\delta\text{-ZrH}}$ and $\{220\}_{\delta\text{-ZrH}}$, more visible in the former.

Turning to the peak positions, Figure 13(b,e) for $\{111\}_{\delta\text{-ZrH}}$, a noticeable increase was first observed at a temperature of $\sim$225 °C, which continued up to final dissolution. After cooling, an increase in final $d_{\{111\}}$ from the original value can be observed, comparable to the observations observed during single cycling. Further cycling resulted in a decrease in $\Delta d_{\{111\}}$ (between heating and cooling), and remained relatively constant for the later cycles. Such shifts were not observed to the same extent for $d_{\{220\}}$, but as noted previously during single cycling, the lattice parameters observed on cooling initially rose, rather than mirroring the on-heating curve.

Figure 13(c,f) tracks the evolution in hydride peak widths. The $\{111\}_{\delta\text{-ZrH}}$ is considered first. On completion of the first cycle, an increase in δ-ZrH$_{\{111\}}$ peak width is observed. After the last cycle, a hysteresis is still shown but to a lesser degree, and a faster increase in peak width on cooling than the decrease on heating can be seen. For the $\{220\}_{\delta\text{-ZrH}}$ peak, widths could be fitted at a higher temperature than in the single-cycle sample shown in Figure 11. Here, across all cycles, a rise in peak width can be observed at the very end of heating, just before complete hydride dissolution. The behaviour on cooling is generally consistent with the $\{111\}_{\delta\text{-ZrH}}$, and single-cycle samples. In addition, the final width at ambient temperatures, once the hydride has fully re-precipitated into the matrix, gradually rose over the course of the four cycles, consistent with $\{111\}_{\delta\text{-ZrH}}$.

3.3.3. Hydride diffraction peak intensity

The azimuthal variation in both $\{111\}_{\delta\text{-ZrH}}$ and $\{0002\}_{\alpha\text{-Zr}}$ diffraction peak intensity has been explored before and after thermomechanical loading (100 MPa) for samples with their tensile axes parallel to both RD and TD. Results are shown in Figure 14. The collected diffraction rings were analysed in 10° azimuthal bins with 0° corresponding to the direction perpendicular to the loading axis. The azimuthal variation in $\{111\}_{\delta\text{-ZrH}}$ intensity, shown for both samples in Figure 14(a,c), is a consequence of the α-Zr texture and the α/δ orientation relationship. It should be recalled that the dominant $\{0002\}_{\alpha\text{-Zr}}$ texture component is found $\sim$ 20° from the ND, towards the TD, and is therefore not sampled by the diffraction measurement around the TD-RD ring. The $\{111\}_{\delta\text{-ZrH}}$ diffraction peak observed near-RD therefore corresponds not to the primary $\{111\}_{\delta\text{-ZrH}}$ parallel to $\{0002\}_{\alpha\text{-Zr}}$ that forms the orientation relationship, but another of the $\{111\}_{\delta\text{-ZrH}}$ family of planes. Nevertheless, changes in the $\{111\}_{\delta\text{-ZrH}}$ intensity variation around the ring may provide indications as to the hydride texture evolution.

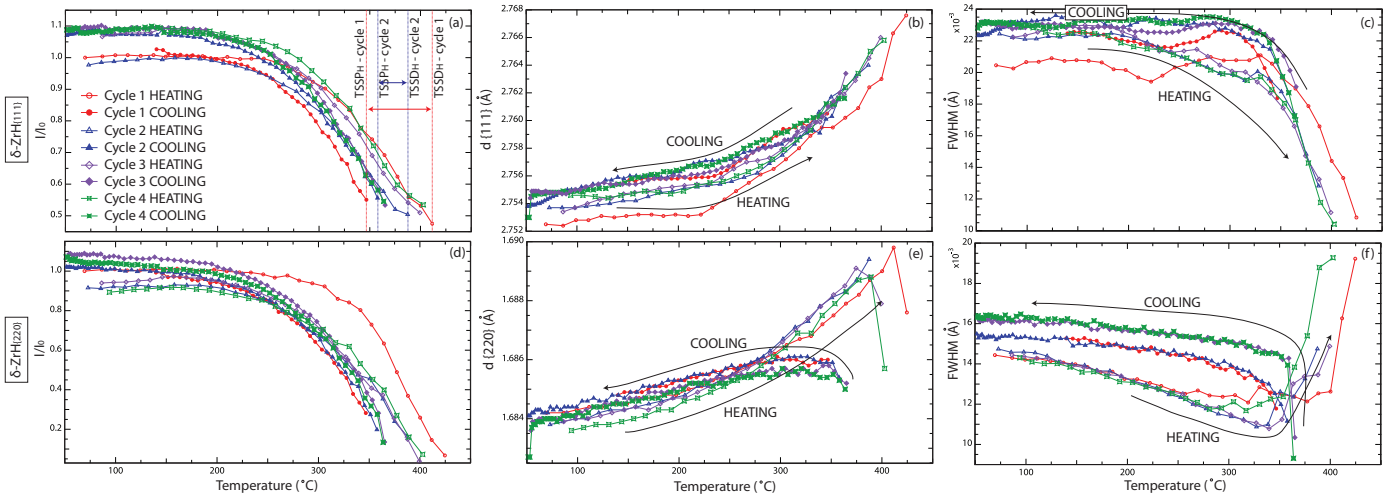

Figure 13: Evolution of the δ-ZrH$_{\{111\}}$ (a-c) and δ-ZrH$_{\{220\}}$ (d-f) peaks near the loading direction ($\pm 10°$), for an RD-loaded sample subjected to a stress of 90 MPa on cooling, over the course of four thermomechanical cycles. The variation in normalised integrated intensity, I/I$_0$ (a,d), peak position, d$_{\{hkl\}}$ (b,e) and peak width, FWHM/1.665 (c,f) are shown.

Considering the TD-aligned sample first, when cooled under a 100 MPa load, additional peaks in the $\{111\}_{\delta\text{-ZrH}}$ peak intensity could be observed at regions corresponding to the sample TD. Turning to consider the orientation relationship, the azimuthal variation in $\{0002\}_{\alpha\text{-Zr}}$ peak intensity before and after loading is shown in Figure 14(b). No change in $\{0002\}_{\alpha\text{-Zr}}$ intensity distribution around the diffraction ring was observed. Similar plots for a sample cooled under a 100 MPa tensile stress parallel to the RD are shown in Figure 14(c,d). Additional peaks in the intensity distribution can, again, be observed, although not in the same sample orientation as shown previously. Consistent with the TD-aligned behaviour, no change in the $\{0002\}_{\alpha\text{-Zr}}$ intensity distribution was observed, indicating no change in α-Zr texture due to loading.

Considering the accompanying BSE micrographs, shown in Figure 7, both the RD and TD aligned samples showed a degree of reorientation during re-precipitation when cooled under a stress of 100 MPa. Originally aligned parallel to the RD, macroscopic hydride packets observed in the RD aligned sample were found to realign themselves 50-60° to the tensile axis. The corresponding intensity distribution plots have also indicated some degree of hydride peak intensity increase at azimuthal angles close to 60° from the loading axis. In contrast, microscopy carried out on the TD-aligned sample showed reorientation in the hydride packet normals from the ND by close to 90° to the TD. The corresponding azimuthal variation in $\{111\}_{\delta\text{-ZrH}}$ peak intensity also showed a slight increase at regions close to the TD, ~90° away from the sample RD. It should be noted that the BSE microscopy highlights the reorientation behaviour of the macroscopic hydride packets relative to the sample ND yet the diffraction data can only consider the microscopic hydride platelet distribution relative to the RD/TD without being able to take into account behaviour along the ND. This is due to the samples' ND running parallel to the incident diffraction beam for all samples.

The evolution in the $\{111\}_{\delta\text{-ZrH}}$ peak intensity around the diffraction ring during four full thermomechanical cycles, cooled under a 90 MPa tensile load, has also been investigated for an RD-aligned sample, Figure 15. Due to the observed symmetry in diffraction peak behaviour around both the RD and TD orientations, a reduced azimuthal range (0-180°) is shown. Figure 15 plots the change in peak intensity distribution for the $\{111\}_{\delta\text{-ZrH}}$ (a) and $\{0002\}_{\alpha\text{-Zr}}$ (b) at the start of cycling and at the end of each separate cycle. No change in $\{0002\}_{\alpha\text{-Zr}}$ intensity distribution was observed across the four cycles. An increase in $\{111\}_{\delta\text{-ZrH}}$ peak intensity at selected azimuthal angles was, however, observed; 30° away from TD, corresponding to 60° from the loading axis. This observation is consistent with data from the single cycle sample. Evidence of increased hydride intensity at alternative azimuthal angles was first noted at the end of cycle one with incremental increases observed upon subsequent cycling.

4. Discussion

Effect of Loading Direction

The degree of reorientation behaviour during a thermomechanical cycle differed depending on the axis of load; parallel to RD or TD. The increased extent of reorientation in the TD sample has been considered a consequence of the parent α-Zr texture, where the majority of grains have their {0002} plane normal slightly tilted towards TD from the plate ND. This implies that a reorientation in the packet morphology from the ND towards the TD requires a less radical change in platelet self-accommodation than a 90° reorientation from the TD-ND plane to the RD.

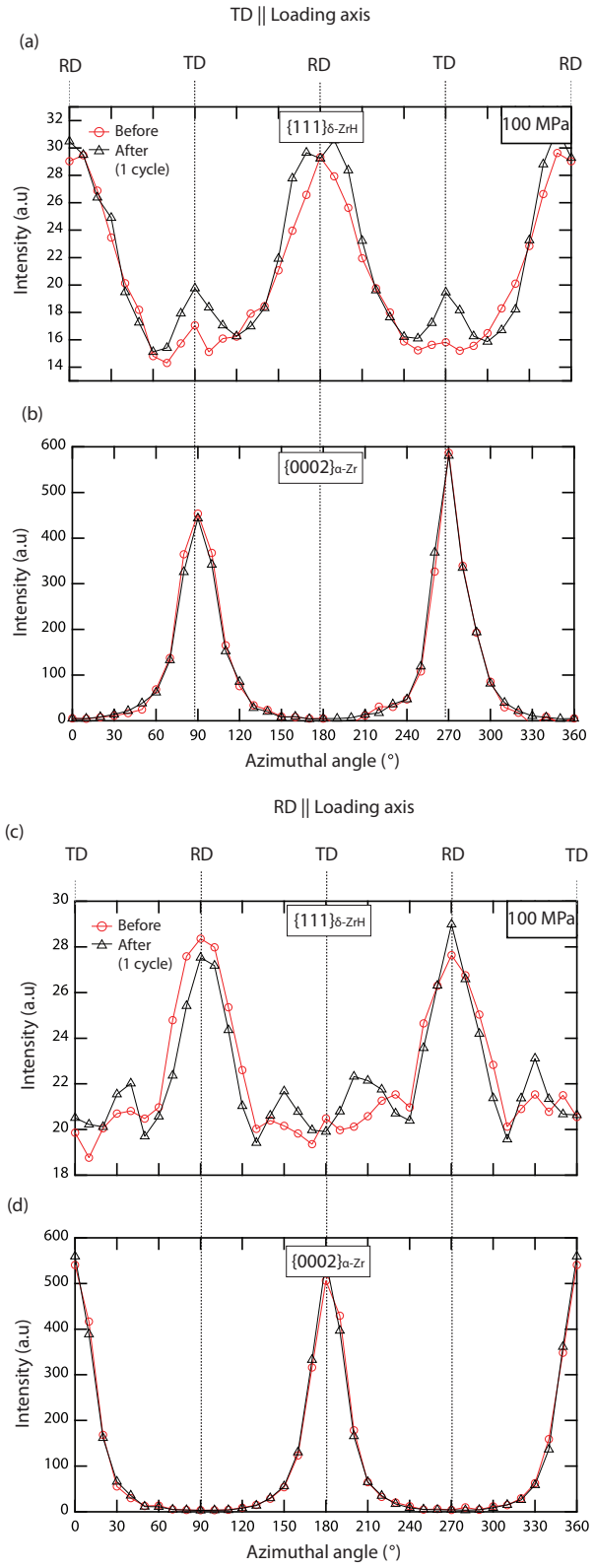

Figure 14: Comparison of intensity plots across the full azimuthal range for the $\{111\}_{\delta\text{-ZrH}}$ (a,c) and $\{0002\}_{\alpha\text{-Zr}}$ (b,d) diffraction peaks before and after a single thermomechanical cycle. (Top) TD-aligned and (Bottom) RD-aligned samples.

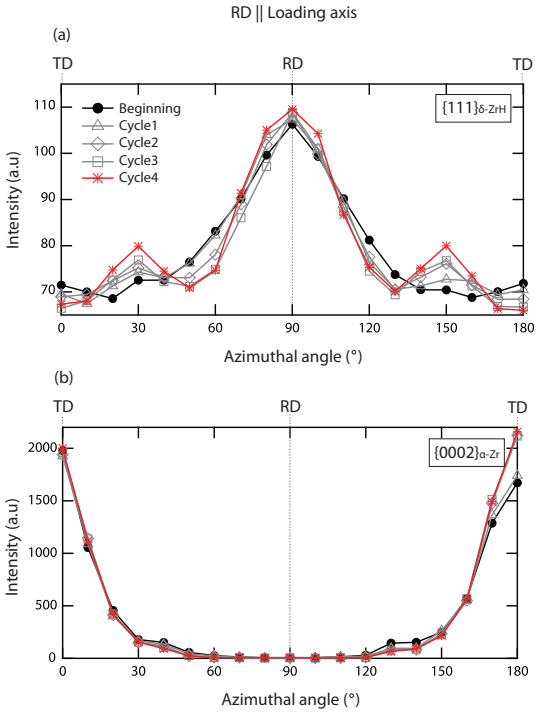

Figure 15: Comparison of intensity plots across a 180° azimuthal range for the $\{111\}_{\delta\text{-ZrH}}$ (a) and $\{0002\}_{\alpha\text{-Zr}}$ (b) diffraction peaks before, during and after four thermomechanical cycles; Loading axis||RD

Evolution in Integrated Intensity

Firstly considering the changes in integrated intensity observed during both single and multiple thermomechanical cycling, the hysteresis on dissolution and re-precipitation, in which the temperature of initial hydride precipitation is notably lower than the point of full dissolution on heating, is considered to be a consequence of the release and re-establishment of misfit accommodation strains[23]. The difference in unit cell volume exhibited by the hydride and matrix phases means that it is necessary to plastically deform the zirconium matrix in order to accommodate a hydride precipitate[23]. Therefore, a significant degree of undercooling (ΔTSS) is required to induce the precipitation of the hydride phase by providing a portion of the energy needed to deform (elastically and plastically) the matrix[24].

The application of multiple thermomechanical cycles, where a tensile stress of 90 MPa was applied on cooling during four identical cycles, was shown to reduce the ΔTSS between heating and cooling, with the largest change observed between cycles one and two. This can be considered in terms of the production of plastic deformation during the application of an external load on cooling at the end of each cycle. According to Birnbaum[25], deformation of the matrix can relieve some of the hydride-matrix misfit strains, aiding the accommodation of the hydride precipi-

tates. By subsequently reducing the amount of undercooling needed, the temperature at which hydrides can form on cooling will therefore be increased. The amount of added plastic deformation induced during subsequent cycles will reduce with each one, a result of stable defect (dislocation) arrangements being established, and so the minimal change in ΔTSS being observed in the later cycles is expected.

Evolution in Lattice Peak Positions

During hydride dissolution and re-precipitation, a distinct change in peak position was observed for the $\{111\}_{\delta\text{-ZrH}}$ for both RD and TD-aligned samples but was not observed to the same extent for the $\{220\}_{\delta\text{-ZrH}}$ peak. An initial steady increase in $\{111\}_{\delta\text{-ZrH}}$ peak position, attributed to constrained thermal expansion, was succeeded by a significant jump to a larger $d_{\delta\text{-}\{111\}}$, considered to be a consequence of the release in hydride-matrix misfit strains. On the contrary, as full hydride dissolution is approached, a smaller increase in $d_{\delta\text{-}\{220\}}$ was observed for samples loaded along the RD and a slight decrease for samples loaded along the TD. This, along with the associated reduction in strain, can be rationalised by appealing to the $\{111\}_{\delta\text{-ZrH}}$ habit plane, with its normal parallel to the α-Zr c-axis. A larger misfit strain along the $[0001]_{\alpha\text{-Zr}}$ when compared to the $[11\bar{2}0]_{\alpha\text{-Zr}}$ has been determined by both Carpenter[26] and Barrow[27]. This gives rise to the characteristic lenticular morphology of the zirconium hydride platelets, with the precipitates' short axis parallel to c, minimising the overall strain energy. As the hydrides dissolve, the release of this (compressive) strain will be greater normal to the $\{111\}_{\delta\text{-ZrH}}$ plane and hence a greater rise in lattice parameter for the $\{111\}_{\delta\text{-ZrH}}$ when compared to the $\{220\}_{\delta\text{-ZrH}}$ was observed. At the end of full hydride precipitation into the matrix, neither $d_{\delta\text{-}\{111\}}$ or $d_{\delta\text{-}\{220\}}$ returned to their original position. This can be indicative of permanent (plastic) strain in the hydrides rather than an effect of the elastic stress from the applied load[17].

Evolution in Peak Width

Considering the observed behaviour between the RD and TD-aligned samples (where the TD sample showed a greater degree of hydride reorientation) the key differences in diffraction data were observed when analysing the $\{111\}_{\delta\text{-ZrH}}$ peak widths. Figure 16 has been produced as a way to rationalise the observed hydride behaviour. On heating, it has been considered that all of the hydride platelets (stacked to appear as macroscopic plates) slowly dissolve together, gradually reducing in size and releasing the associated hydride-matrix misfit strains, Figure 16(c). This will cause a decrease in peak width (a) and increase in lattice parameter, $d_{\delta\text{-}\{111\}}$(b). The observed changes in associated strain are quite large; 0.015Å corresponds to a strain of $\Delta d/d \simeq 0.5\%$ and a stress of ∼0.76 GPa but similarly large strains have been seen by both Colas[17] and Barrow[27]. It should also be recalled that these values correspond to local strains in the vicinity of nanoscale precipitates and so stresses in excess of macroscopic yield are possible. At the point of initial formation in the matrix, the precipitate will be highly constrained, with no relief of stress by associated plastic deformation/lattice defects. A large strain on the hydride platelets will therefore be applied by the matrix and, once a sufficient hydride volume fraction is reached allowing them to interact, will be associated by a large initial $\{111\}_{\delta\text{-ZrH}}$ diffraction peak width. This is much greater than the value noted just prior to full dissolution on heating as the hydrides are far less constrained due to their reduced size. The strain field surrounding the precipitate can then provide the nucleation site for adjacent platelets to initiate and grow, in a manner consistent with an autocatalytic nucleation process where arrays of crystallographically related product phases are formed[28]. When a load is applied, a similar situation obtains, but the packet morphology changes, owing to the accommodation of the applied stress. As suggested by Colas et al[29], the suppression of circumferential hydride precipitation due to an applied stress can enable hydrides to precipitate in different orientations.

The orientation of the individual hydride platelets is generally considered to be maintained and hence the intensity of the diffraction peaks, across the 20° azimuthal

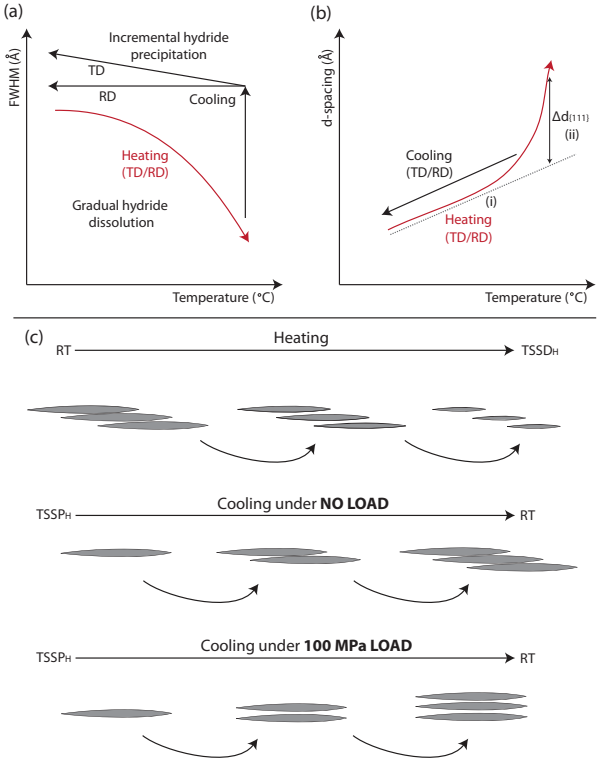

Figure 16: Schematic representation of the observed evolution in (a) peak width, FWHM and (b) peak position, $d_{\{111\}}$ during thermomechanical cycling, together with the suggested evolution in the packet morphology (c).

range (±10° about loading axis) considered, is also (generally) maintained. The altered packet morphology gives rise to different accommodation stresses and strains between the platelets with notably increased strain accumulation observed for the sample aligned along the TD during cycling. The corresponding increase in peak broadening for the TD aligned sample (exhibiting a larger degree of packet reorientation) can be considered in terms of an increase in plastic strain, perhaps due to the build up of dislocations. A reduction in strain accommodation within the matrix is associated with hydride precipitation when in their reoriented morphology when compared to the naturally precipitated packets giving rise to increases in peak width.

Hydride Behaviour during Multiple Cycles
Considering the overall behaviour across all four cycles with respect to peak intensity, peak position and peak width (Figure 13), the majority of changes were observed between cycles one and two, with the behaviour generally remaining constant for subsequent cycles. This, as previously suggested, could be interpreted in a way that suggests the majority of packet reorientation behaviour (microscopic platelets generally retain their established orientation relationship with the α-Zr) occurs during the the earlier cycles, with minimal changes observed during the later ones. The accompanying BSE micrographs from the RD-aligned sample comparing hydride morphology after a single thermomechanical cycle, Figure 12, provided further evidence to suggest that, under the conditions analysed, the majority of packet realignment occurred during the early cycles with very little difference observed between the two.

Change in Azimuthal Hydride Distribution with Thermomechanical Cycling
It has been shown that the application of thermomechanical loads can, to some degree, alter the microscopic hydride platelet distribution, Figures 14 and 15, evident from an increase in $\{111\}_{\delta\text{-ZrH}}$ diffraction peak intensity at different azimuthal angles after loading. Initially considering the hypothesis that this was due to a change in α-Zr texture, the azimuthal variation in $\{0002\}_{\alpha\text{-Zr}}$ peak intensity around 180° (owing to the symmetry of the sample) was assessed and compared to the variation in $\{111\}_{\delta\text{-ZrH}}$ peak. No noticeable difference in the $\{0002\}_{\alpha\text{-Zr}}$ intensity distribution could be seen leading to the assumption that the starting α-Zr texture was fully retained during loading.

Hydride precipitation is often considered in terms of their nucleation energy and their tendency to precipitate at regions with the smallest nucleation barrier. Their first stage of nucleation into the α-Zr lattice (in this case when cooled from a temperature above the terminal solid solubility for the concentration of hydrides) is considered crucial when determining their orientation with Ells[30] concluding that the preferential orientation of hydride packets is most efficient during nucleation rather than through growth of a stable nuclei. The application of a tensile stress during hydride re-precipitation from solution may change the preferential sites for hydride formation by reducing the energy barrier for nucleation. Work done by Vizcaino[31] on Zr-2.5%Nb pressure tube material showed that hydride precipitation preferentially occurs in grains oriented in two ideal orientations; (i) c-axis parallel to the hoop direction (m_{hoop}) and (ii) c-axis parallel to an intermediate direction (m_{tilted}). When thermally cycled under a load, the values for hydrogen solubility for both orientations changed; hydride dissolution and precipitation temperatures for m_{tilt} α-Zr grains were ∼5-15° higher than m_{hoop} grains and was accompanied by a redistribution of hydrides in particular grain orientations. Similar behaviour has been postulated to occur during this study. The redistribution of hydrides differed depending on the axis of loading, where TD-loaded samples showed more drastic reorientation behaviour than those loaded along the RD. This could suggest that loading along different directions during cooling can reduce the energy barrier for hydride nucleation for different sets of oriented α-Zr grains.

5. Conclusions

Diffraction experiments have been performed examining the reorientation behaviour of zirconium hydride during the thermomechanical cycling of Zircaloy-4 plate material. The following conclusions can be drawn.

1. Reorientation of the macroscopic hydride packets from the normal direction, with the $\{111\}_{\delta\text{-ZrH}}$ habit plane parallel to the dominant $\{0002\}_{\alpha\text{-Zr}}$ texture, was observed to be much more significant when loaded along the transverse direction than the rolling direction.
2. Reorientation when loading along the rolling direction resulted in a greater proportion of hydride packets of a mixed morphology, whilst loading along the transverse direction resulted in the majority being in a so-called 'radial' morphology (hydride packet traces angled 0-40° from the sample ND).
3. Evidence of small changes in hydride crystallographic texture with reorientation was observed. For the $\{111\}_{\delta\text{-ZrH}}$ peak, regions of elevated intensity ∼50-60° from the tensile axis were observed when loaded along the sample RD whereas when loaded along the sample TD, regions of increased intensity were observed ∼90° from the tensile axis. Both were cooled under a load of 100 MPa.
4. A decrease in $\{111\}_{\delta\text{-ZrH}}$ peak width and increase in $\{111\}_{\delta\text{-ZrH}}$ lattice parameters were observed during dissolution. Steeper change in both peak width and $d_{\{111\}}$ were observed on cooling, behaviour which has been attributed to the difference between gradual dissolution on heating and sympathetic nucleation on cooling of the individual microscopic platelets that make up the macroscopically-observed hydride packet stringers.

5. The hysteresis in hydride dissolution and re-precipitation was observed to decrease on repeated thermal cycling.

Acknowledgements

The provision of material by Ted Darby at Rolls-Royce plc is acknowledged, along with assistance with the funding of HEW. Time at I12 beamline at the Diamond synchrotron was provided by STFC. EPSRC provided funding for HEW, NGJ and DD (EP/H004882/1). The assistance of O Joris, A Radecka, P Tympel, and T Connolley is also gratefully acknowledged.

References

[1] J. J. Kearns, Terminal Solubility and Partitioning of Hydrogen in the Alpha Phase of Zirconium, Zircaloy-2 and Zircaloy-4, Journal of Nuclear Materials 22 (1967) 292–303.

[2] W. Goll, H. Spilker, E. H. Toscano, Short-time creep and rupture tests on high burnup fuel rod cladding, Journal of Nuclear Materials 289 (3) (2001) 247–253.

[3] K. B. Colas, A. T. Motta, J. D. Almer, M. R. Daymond, M. Kerr, In Situ Study of Hydride Precipitation Kinetics and Re-orientation in Zircaloy using Synchrotron Radiation, Acta Materialia 58 (2010) 6575–6583.

[4] K. Sakamoto, M. Nakatsuka, Stress Reorientation of Hydrides in Recrystallized Zircaloy-2 Sheet, Journal of Nuclear Science and Technology 43 (9) (2006) 1136–1141.

[5] D. O. Northwood, U. Kosasih, Hydrides and Delayed Hydrogen Cracking in Zirconium and its Alloys, International Metals Reviews 28 (2) (1983) 92–121.

[6] J. B. Bai, N. Ji, D. Gilbon, C. Prioul, D. Francois, Hydride Embrittlement in Zircaloy-4 Plate: Part II. Interaction Between the Tensile Stress and the Hydride Morphology, Metallurgical and Materials Transactions A 25A (1994) 1199–1208.

[7] D. Hardie, M. W. Shanahan, Stress Reorientation of Hydrides in Zirconium-2.5% Niobium, Journal of Nuclear Materials 55 (1975) 1–13.

[8] R. N. Singh, R. Kishore, S. S. Singh, T. K. Sinha, B. P. Kashyap, Stress-Reorientation of Hydrides and Hydride Embrittlement of Zr–2.5 wt% Nb Pressure Tube Alloy, Journal of Nuclear Materials 325 (1) (2004) 26–33.

[9] M. Leger, A. Donner, The Effect of Stress on Orientation of Hydrides in Zirconium Alloy Pressure Tube Materials, Canadian Metallurgical Quarterly 24 (3) (1985) 235–243.

[10] Y. Mishima, T. Okubo, Effect of Thermal Cycling on the Stress Orientation and Circumferential Ductility in Zircaloy-2, Canadian Metallurgical Quarterly 11 (1) (1972) 157–164.

[11] H. C. Chu, S. K. Wu, R. C. Kuo, Hydride Reorientation in Zircaloy-4 Cladding, Journal of Nuclear Materials 373 (2008) 319–327.

[12] B. A. Cheadle, C. E. Coleman, Orientation of Hydrides in Zirconium Alloy Tubes, Zirconium in the Nuclear Industry: Sixth International Symposium, ASTM STP 824, ASTM Int'l, West Conshohocken, PA, USA (1984) 210–221.

[13] J. J. Kearns, C. R. Woods, Effect of Texture, Grain Size, and Cold Work on the Precipitation of Oriented Hydrides in Zircaloy Tubing and Plate, Journal of Nuclear Materials 20 (1966) 241–261.

[14] J. S. Bradbrook, G. W. Lorimer, N. Ridley, The Precipitation of Zirconium Hydride in Zirconium and Zircaloy-2, Journal of Nuclear Materials 42 (1972) 142–160.

[15] K. Une, K. Nogita, S. Ishimoto, K. Ogata, Crystallography of Zirconium Hydrides in Recrystallized Zircaloy-2 Fuel Cladding by Electron Backscatter Diffraction, Journal of Nuclear Science and Technology 41 (7) (2004) 731–740.

[16] Y. S. Kim, Y. Perlovich, M. Isaenkova, S. S. Kim, Y. M. Cheong, Precipitation of Reoriented Hydrides and Textural Change of α-Zirconium Grains during Delayed Hydride Cracking of Zr–2.5%Nb Pressure Tube, Journal of Nuclear Materials 297 (3) (2001) 292–302.

[17] K. B. Colas, A. T. Motta, M. R. Daymond, M. Kerr, Hydride Platelet Reorientation in Zircaloy Studied with Synchrotron Radiation Diffraction, Journal of ASTM International 8 (1) (2011) 1–16.

[18] B. A. Cheadle, C. E. Ells, W. Evans, The Development of Texture in Zirconium Alloy Tubes, Journal of Nuclear Materials 23 (1967) 199–208.

[19] O. N. Pierron, D. A. Koss, A. T. Motta, K. S. Chan, The Influence of Hydride Blisters on the Fracture of Zircaloy-4, Journal of Nuclear Materials 322 (2003) 21–35.

[20] P. A. Raynaud, D. A. Koss, A. T. Motta, K. S. Chan, Fracture Toughness of Hydrided Zircaloy-4 Sheet Under Through-Thickness Crack Growth Conditions, Journal of ASTM International 5 (2007) 1–15.

[21] P. A. Raynaud, D. A. Koss, A. T. Motta, Crack Growth in the Through-Thickness Direction of Hydrided Thin-Wall Zircaloy Sheet, Journal of Nuclear Materials 420 (1-3) (2012) 69–82.

[22] A. McMinn, E. C. Darby, J. S. Schofield, The Terminal Solid Solubility of Hydrogen in Zirconium Alloys, Zirconium in the Nuclear Industry: Twelfth International Symposium, ASTM STP 1354 (2000) 173–195.

[23] M. P. Puls, Elastic and Plastic Accommodation Effects on Metal-Hydride Solubility, Acta Metallurgica 32 (8) (1984) 1259–1269.

[24] M. P. Puls, The Effects of Misfit and External Stresses on Terminal Solid Solubility in Hydride-Forming Metals, Acta Metallurgica 29 (12) (1981) 1961–1968.

[25] H. K. Birnbaum, M. L. Grossbecr, M. Amano, Hydride Precipitation in Nb and Some Properties of NbH, Journal of the Less Common Metals 49 (1976) 357–370.

[26] G. Carpenter, The Dilatational Misfit of Zirconium Hydrides Precipitated in Zirconium, Journal of Nuclear Materials 48 (1973) 264–266.

[27] A. Barrow, A. Korinek, M. R. Daymond, Evaluating Zirconium–Zirconium Hydride Interfacial Strains by Nano-Beam Electron Diffraction, Journal of Nuclear Materials 432 (2013) 366–370.

[28] V. Perovic, G. C. Weatherly, C. J. Simpson, The Role of Elastic Strains in the Formation of Stacks of Hydride Precipitates in Zirconium Alloys, Scripta Metallurgica 16 (1982) 409–412.

[29] K. B. Colas, A. T. Motta, M. R. Daymond, J. D. Almer, Effect of thermo-mechanical cycling on zirconium hydride reorientation studied in situ with synchrotron X-ray diffraction, Journal of Nuclear Materials 440 (1-3) (2013) 586–595.

[30] C. E. Ells, The Stress Orientation of Hydride in Zirconium Alloys, Journal of Nuclear Materials 35 (1970) 306–315.

[31] P. Vizcaino, J. R. Santisteban, M. Alvarez, Effect of Crystallite Orientation and External Stress on Hydride Precipitation and Dissolution in Zr2.5%Nb, Journal of Nuclear Materials 447 (2014) 82–93.